Earth and Planetary Science Letters 295 (2010) 487–496

Contents lists available at ScienceDirect

Earth and Planetary Science Letters

journal homepage: www.elsevier.com/locate/epsl

Metal–silicate silicon isotope fractionation in enstatite meteorites and constraints on Earth's core formation

Karen Ziegler [a,b,*], Edward D. Young [a,b], Edwin A. Schauble [b], John T. Wasson [a,b]

[a] Institute of Geophysics and Planetary Physics, 603 Charles Young Drive East, 3845 Slichter Hall, Box 951567, University of California Los Angeles, Los Angeles, CA 90095-1567, USA
[b] Department of Earth and Space Sciences, 595 Charles Young Drive East, 3806 Geology Building, Box 951567, University of California Los Angeles, Los Angeles, CA 90095-1567, USA

ARTICLE INFO

Article history:
Received 12 September 2009
Received in revised form 8 April 2010
Accepted 16 April 2010
Available online 23 May 2010

Editor: R.W. Carlson

Keywords:
silicon isotope fractionation
metal
silicate
enstatite meteorite
Bulk Silicate Earth
Earth's core formation

ABSTRACT

Silicon has long been considered a possible light element in Earth's core. If differences in $^{30}Si/^{28}Si$ ratios between metal (core) and silicate (mantle and crust) can be quantified, silicon isotopes may be used to constrain the amount of this element in the core, and in so doing elucidate the conditions that attended Earth's differentiation. We investigate Si-isotope fractionation between metal and silicate in metal-rich enstatite meteorites as an analogue for Earth's differentiation. We report here a 5 to 6‰ difference in the $^{30}Si/^{28}Si$ ratio between Si in metal and Si in silicate in the aubrites (enstatite achondrites) Mount Egerton and Norton County. The meteorites are believed to have derived from enstatite chondrites by melting and thermal metamorphism with final equilibration at 1200 and 1130 ± 80 K, respectively. Using the measured silicate–metal Si-isotope fractionation in these rocks we obtain a temperature dependence for fractionation of $\Delta^{30}Si_{\text{silicate-metal}} = \frac{7.64 \times 10^6 \pm 0.47(1\sigma)}{T^2}$, in agreement with independent experimental and theoretical determinations. The measured silicate–metal fractionation suggests a ~0.8‰ difference in the $^{30}Si/^{28}Si$ ratio between Earth's core and mantle at *P/T* conditions relevant to core formation. Our results, based on thermodynamic calculations for Si solubility in iron-rich metal and the measured Si-isotopic silicate–metal fractionation, imply at least ~6 wt.% Si in the core (depending on the exact $\Delta^{30}Si_{\text{BSE-chondrite}}$ value). The Si-isotope data also require that oxygen fugacity in the lower mantle increased during or after the process of core segregation by 1 to 2 log units.

1. Introduction

Earth's core exhibits a 5 to 10% deficit in density based on seismic velocities, requiring the presence of elements less dense than pure Fe–Ni alloy (Birch, 1964). Candidate elements include carbon, hydrogen, sulfur, silicon, and oxygen, but it was long ago suggested that Si may be the principal low-density diluent (Ringwood, 1959). Differences in $^{30}Si/^{28}Si$ ratios between Bulk Silicate Earth (BSE) and meteorites can constrain the amount of Si in Earth's core if silicon isotope partitioning between silicate and metal can be quantified (Georg et al., 2007). Here we use results from enstatite meteorites to quantify the silicate–metal fractionation of silicon isotopes.

Equilibration between Earth's core and mantle is thought to have occurred near the base of a silicate magma ocean as molten Fe coalesced to form an immiscible liquid of Fe–Ni metal (Javoy, 1995; Wade and Wood, 2005; Wood, 2008; Frost et al., 2008). The molten metal is expected to have sunk to the base of the less dense magma (e.g., Wade and Wood, 2005). Pressures and temperatures at the base of the magma ocean are estimated to have been ~40 GPa and ~3000 K (Zerr et al., 1998; Wood, 2008). The presence of silicon in Earth's core has important implications for conditions attending core segregation. Silicon in the core suggests low oxygen fugacity (f_{O_2}) during core formation by the schematic reaction $SiO_2 + 2Fe_{metal} = Si_{metal} + 2FeO$. Incorporation of Si into molten iron metal depends primarily on temperature (*T*) and f_{O_2}, with a smaller but uncertain pressure (*P*) dependency (e.g., Gessmann et al., 2001; Malavergne et al., 2004; Mann, 2007). Most of any Si that may have entered the metal during segregation can be assumed to have remained in the core (Gessmann et al., 2001). Oxygen fugacity during core formation is believed to have been lower than that exhibited by the lower mantle today (Wade and Wood, 2005), and would be well constrained by a determination of the amount of Si in the core.

Differences in $^{30}Si/^{28}Si$ ratios between Si in silicate and Si in Fe-rich metal are expected because of the very different bonding environments of Si in these two phases. At equilibrium, silicon in silicate should have a higher $^{30}Si/^{28}Si$ ratio than Si in metal (Schauble, 2004). If significant quantities of Si are present in Earth's core, the loss of Si with low $^{30}Si/^{28}Si$ ratio should have left the silicate portion of Earth with a high $^{30}Si/^{28}Si$ ratio compared with the isotopic composition of the planet as a whole. The mass-balance relationship between the

* Corresponding author. Institute of Geophysics and Planetary Physics, 603 Charles Young Drive East, 3845 Slichter Hall, Box 951567, University of California Los Angeles, Los Angeles, CA 90095-1567, USA. Tel.: +1 310 794 4484; fax: +1 310 206 3051.
E-mail addresses: kziegler@ess.ucla.edu (K. Ziegler), eyoung@ess.ucla.edu (E.D. Young), schauble@ucla.edu (E.A. Schauble), jtwasson@ucla.edu (J.T. Wasson).

0012-821X/$ – see front matter © 2010 Elsevier B.V. All rights reserved.
doi:10.1016/j.epsl.2010.04.030

silicon-isotopic composition of the BSE, the silicon-isotopic composition of the whole planet, and the fraction of Earth's silicon that resides in the core is

$$\delta^{30}Si_{BSE} - \delta^{30}Si_{chondrite} = \Delta^{30}Si_{silicate-metal} f_{Si,core} \quad (1)$$

where $f_{Si,core}$ is the fraction of Earth's silicon in the core, $\delta^{30}Si_i$ refers to the permil difference between the $\delta^{30}Si$ value in reservoir i from the $\delta^{30}Si$ value of NBS-28 reference material, and $\Delta^{30}Si_{silicate-metal} \equiv \delta^{30}Si_{silicate} - \delta^{30}Si_{metal}$. Eq. (1) assumes that bulk Earth (BSE plus core) has a chondritic $\delta^{30}Si$ value. Eq. (1) underscores that the $\Delta^{30}Si_{silicate-metal}$ value must be known in order to use $\Delta^{30}Si_{BSE\text{-}chondrite}$ as indicator of Si in the core. At present, there are theoretical predictions (Georg et al., 2007) and an experimental datum (Shahar et al., 2009) suggesting a relationship between temperature and the $\Delta^{30}Si_{silicate-metal}$ value, but no instances of the effect in natural rocks have been reported.

Here we present the first measured $\Delta^{30}Si_{silicate-metal}$ values for natural systems. The materials we chose are aubrites, meteorites evolved from enstatite chondrites (E chondrites) by processing at high temperatures. E chondrites are sometimes regarded as analogues for Earth prior to differentiation. They are the only primitive meteorite group with oxygen isotope compositions and metal-to-silicate ratios similar to those of Earth (Mayeda and Clayton, 1980; Herndon, 1996; Newton et al., 2000). They are among the most reduced rocks known, with most of their iron comprising metal or sulfide rather than oxide and Si concentrations in metal of up to ~5 wt.% (Ringwood, 1961; Humayun et al., 2009). Silicon isotope partitioning between metal and silicate in enstatite meteorites affords a proxy for the early stages of Earth's core formation when the intrinsic f_{O_2} is thought to have been lower than that in the mantle today (Wade and Wood, 2005).

2. Samples and methods

Silicon isotopes were measured by employing two different extraction techniques on the front end of a ThermoFinnigan Neptune™ multiple-collector inductively coupled plasma-source mass spectrometer (MC-ICPMS). These techniques are: (1) Si extraction by acid digestion followed by ion-exchange purification and analysis in solution in dry plasma mode (Cetac Aridus™); and (2) Si extraction by laser ablation using a Photon Machines Analyte™ 193 nm excimer laser with a <4 ns pulse length.

2.1. Samples

The main targets of this study are the Mount Egerton meteorite (USNM 5320), classified as an anomalous aubrite (enstatite achondrite), and the Norton County meteorite (UNM 576), an aubrite.

Mount Egerton is unbrecciated and has a relatively high metal content (McCall, 1965; Casanova et al., 1993a). Its major phase is silicate, consisting almost exclusively of cm-sized enstatite grains ($Wo_{0.80}En_{99.11}Fs_{0.09}$), with traces of diopside ($Wo_{44.7}$). Troilite and schreibersite are minor phases (Wasson and Wai, 1970; Watters and Prinz, 1979; Watters and Prinz, 1980; Watters et al., 1980). The metal comprises 21 wt.% of the bulk meteorite, occurs mostly as large cm-sized blobs, and consists of 97.8 wt.% kamacite (2.1 wt.% Si) and 2.2 wt.% perryite (a nickel-silicide, 11.8 wt.% Si) (Wai, 1970; Wasson and Wai, 1970; Casanova et al., 1993a), suggesting a Si concentration of 2.3 wt.% for the bulk metal. From the given references we calculate concentrations of 4.5 mol% of Si in metal, and 0.008 mol% Fe in enstatite.

Norton County is a brecciated aubrite, and is composed largely of large enstatite crystals ($Wo_{0.5-1.2}En_{98.8-99.5}$) with traces of diopside ($Wo_{40.1-46.1}$), forsterite and plagioclase (Watters and Prinz, 1979; Okada et al., 1988). Metal occurs in irregular shapes, and comprises 1–1.5 vol.% of the meteorite. The metal is kamacite (0.91 wt.% Si), 1.4 to 2.0 wt.% perryite (10.3 wt.% Si), and up to 5.7 wt.% schreibersite (0.1 wt.% Si) (Wasson and Wai, 1970; Watters and Prinz, 1979; Casanova et al., 1993b). Average concentrations of 2.1 mol% of Si in metal and 0.008 mol% Fe in enstatite were calculated for Norton County.

Reactions involving oxidized and reduced forms of Si and Fe can be used to infer equilibration temperatures for reduced meteorites (Larimer, 1968; Wasson et al., 1994). The calibration of Si and Fe partitioning between metal and silicate of Wasson et al. (1994) applied to the above phase compositions yields equilibration temperatures of 1200 K and 1130 K for Mount Egerton and Norton County, respectively. Wasson et al. (1994) suggest an uncertainty of ± 80 K for this calibration due to uncertainties in the activity coefficient and Gibbs free energies of reaction.

The meteorites Abee and Indarch are classified as EH4 chondrites. Abee is a breccia consisting of equal proportions of clasts and matrix, kamacite nodules, and sulfides. Due to its brecciated nature, major differences in mineral abundances exist in different areas of the meteorite (total silicates ~30 to 65 wt.%, total metal ~20 to 40 wt.%). The silicate phase consists dominantly of enstatite, with lower abundances of silica and albite (Rubin and Keil, 1983; Rubin and Scott, 1997). Indarch contains ~18 wt.% metal (kamacite), ~10 wt.% sulfides, with the remaining silicate phase being dominated by enstatite (Keil, 1968).

The sample of the Murchison meteorite (CM2 carbonaceous chondrite) is from the UCLA meteorite collection.

We analyzed four different aliquots of terrestrial olivine, all of which are from the San Carlos (SC) ultramafic site. One aliquot is from a large volume of SC olivine distributed by Stein Jacobsen (Harvard University), one is a USNM sample (136718), and two others are SC olivines from batches available at UCLA.

2.2. Sample preparation by wet chemistry

2.2.1. Phase separation

The silicate and metal phases of Mount Egerton and Norton County were separated by breaking apart large (~1 cm) grains of enstatite and metal, followed by ultrasonication in ultrapure water to remove attached impurities. Microscopic inspection showed no metal on the separated enstatite, and no enstatite on the metal. Metal in Indarch and Abee is finely disseminated throughout the rock. For silicate separation, metal particles were removed from the finely crushed whole rocks by a hand magnet, followed by microscopic inspection. Due to the difficulty of obtaining clean metal separates from Indarch and Abee (and the large isotope effect silicate contamination can imprint), the metal phases were not analyzed for these rocks. The metal-free Murchison was crushed in bulk.

2.2.2. Sample dissolution

Silicate samples and standards (NBS-28; IRMM-018a, Diatomite, BigBatch, (Reynolds et al., 2007); SC olivine) were dissolved in 2.5 M ultrapure HF at ~120 °C in sealed Teflon Savillex™ beakers. The volume of 2.5 M HF used is dictated by the Si concentration of the silicate, and a final target concentration of fluosilicate ions below 40 mM, in order to avoid volatilization of SiF_4. Concentrated ultrapure HNO_3 was added to accelerate dissolution in stubborn cases without adding additional F^- ions. This dissolution method has been shown to achieve full recovery and not to induce any Si isotopic fractionation (De La Rocha et al., 1996). Any possible trace contamination of metal would not affect the silicate Si as metal does not dissolve in HF. The Si solutions were diluted to obtain a 4.6 ppm Si solution containing 0.02% HF. Isotopic fractionation due to polymerization reactions, has been reported for solutions of pH values <2 loaded onto cation exchange columns, whereas solutions of a pH of 2–3 did not show fractionation (Fitoussi et al., 2009). Our solutions have a final pH of 2.0.

Metal samples were dissolved in concentrated ultrapure HCl to yield Fe in solution and a silica gel according to the simplified reactions:

$$FeSi_s + 6HCl_{aq} \rightarrow FeCl_{2aq} + SiCl_{4aq} + 3H_2$$

$$SiCl_{4aq} + 2H_2O \rightarrow SiO_{2gel} + 4HCl_{aq}$$

where the second reaction is so rapid as to preclude loss of Si as volatile $SiCl_4$ (Bauer and Deiss, 1915). Solutions were dried down at 100 °C, and the recovered silica gel dissolved in 2.5 M HF as described above. These solutions have a final pH of 2.0 to 2.2.

2.2.3. Silicon separation

Purification of Si was achieved by ion-exchange chromatography following the method described by Georg et al. (2006). We used columns with 2 ml of BioRad cation exchange resin DOWEX 50W-X12 (200–400 mesh) in H^+ form. Column loads consist of 3.6 µg of Si in 0.02% HF, and Si is eluted with 4 ml of MQ-e water (pH neutral, 18.5 MΩ), while the resin retains all ambient cationic species. The resulting solution has final concentrations of Si and HF of ~0.5 ppm and 0.002%, respectively. Elution curves for silicates and metal show full recovery of all Si. The Si-isotopic ratios from pure Si solutions (see Section 2.5) before and after the column purifications are identical, and are taken as the most sensitive indicator of complete yield.

In preparation for isotopic analyses, the column elutes (Si in 0.002% HF) were spiked with concentrated HNO_3 to obtain a 2% HNO_3 solution. Special attention was paid to precisely match the acid matrix of the standard solutions (2% HNO_3, 0.002% HF), as mismatches in HF concentrations on the order of 100% (e.g., 0.002% vs. 0.004%) cause shifts in measured δ^{30}Si values of up to 0.1‰. We find that 0.002% HF has neither a measurable isotopic matrix effect, nor does it induce signal instability (noticeable at concentrations above 0.2%).

2.3. Laser ablation

For laser-ablation analyses, Si was extracted from silicate by *in-situ* ablation to form pits 52 to 69 µm in diameter at a pulse repetition rate of 3–6 Hz, and from metal by ablation of 172 µm pits at 6–12 Hz. UV fluence was 19 J/cm^2. Laser-ablation products were carried from the sample chamber to a mixing volume by Helium (0.51 l/min) where it was combined with dry Ar gas (0.69 l/min), and then introduced into the ICP-torch.

2.4. Mass spectrometry

Solution samples were run in dry plasma mode using the Cetac Aridus™ I desolvating system, the Cetac PFA microconcentric Aspire™ nebulizer with a 50 µl/min uptake rate, and a PFA spray chamber. We measure $^{28}Si^+$, $^{29}Si^+$, and $^{30}Si^+$ intensities simultaneously. Ion beam intensities for ~0.5 ppm solutions were between 150 and 200 mV on $^{29}Si^+$, with backgrounds of <5 mV. The presence of 0.002% HF in the solution and the use of a glass torch body did not add measurably to the normal Si background signal. The MC-ICPMS was operated at a mass resolving power (instrumental $m/\Delta m$) of ~12,000. High mass resolution eliminates potential molecular interferences from $^{28}N_2^+$ and $^{12}C^{16}O^+$ for $m/z=28$, $^{14}N^{15}N^+$ and $^{12}C^{17}O^+$ for $m/z=29$, and $^{14}N^{16}O^+$ and $^{12}C^{18}O^+$ for $m/z=30$. Potential doubly-charged mass interference species and their first ionization potentials include $^{56}Fe^{2+}$ (m/z~28, 16.18 eV), $^{58}Ni^{2+}$ (m/z~29, 18.15 eV), $^{58}Fe^{2+}$ (m/z~29, 16.18 eV), and $^{60}Ni^{2+}$ (m/z~30, 18.15 eV). These doubly-ionized species have first ionization potentials greater than that of Ar^+ (15.76 eV), with the result that they are not detectable in our mass spectra for the solution work (c.f. laser ablation of metals, see below). Corrections for instrumental mass bias (~5%) were performed by sample-standard bracketing with peak height matching between sample and standard to <5%. Solutions were measured in blocks of 20 cycles with ~4 s integrations per cycle; a typical analysis comprises 10 blocks of 20 cycles. Internal precision for the measurements is usually better than ±0.2‰ (2se) per amu for δ^{30}Si, but often <0.1‰. The external reproducibility of our in-house standard taken through the column chemistry with a typical silicate matrix is <0.1‰.

For laser-ablation analyses, the MC-ICPMS was operated at medium resolution with mass resolving power of ~7000. At this resolution it is possible for some doubly-charged species of abundant Ni and Fe to cause interferences at Si cardinal masses, high ionization potentials of the former notwithstanding. For example, $m/\Delta m$ for $^{58}Ni^{++}$ and $^{29}Si^+$ is ~3200, suggesting an instrumental $m/\Delta m$ of >9000 would be required to resolve these species. Indeed, we find that ablation of Fe–Ni-metals with very low concentrations of Si results in interferences from the doubly-charged species $^{56}Fe^{++}$ (m/z~28), $^{58}Ni^{++}$ and $^{58}Fe^{++}$ (m/z~29), and $^{60}Ni^{2+}$ (m/z~30) at the mass resolution of our measurements. These interferences manifest as spurious mass-independent isotope fractionation effects, i.e. $\Delta^{29}Si = \delta^{29}Si - 0.518 \times \delta^{30}Si$ values deviating from zero. To circumvent this, we obtained preceding on-peak blanks for Si in metal by ablating Si-free Fe–Ni-metal (metal from the Esquel pallasite). This procedure eliminated or reduced mass interference effects from Ni and Fe. In a few cases, however, non-zero Δ^{29}Si values in excess of our precision persisted, which was understood to be due to variations in, and differences between, the Fe:Ni-ratios of the samples and blanks. We used the Δ^{29}Si value as a criterion for reliability; analyses with absolute values of $\Delta^{29}Si > 0.12$‰ were rejected.

Measurements were done in blocks of 11 cycles with ~4 s integrations per cycle. Internal precision for Si-isotope ratios obtained by laser ablation is <0.3‰ (2se) for δ^{30}Si. Calibration was accomplished by laser-ablation analyses of the international Si-isotope standard IRMM-18a and our in-house standard (USNM 136718 olivine) against NBS-28. Therefore, the Si-isotope data obtained by laser ablation are completely independent of the data obtained by solution, i.e., no cross-referencing or cross-calibration between the two techniques was involved.

2.5. Testing the isotope fidelity of wet-chemical extraction and purification

In order to verify the isotopic fidelity of our wet-chemistry procedures, we conducted a number of tests that are described in detail in Shahar et al. (2009) (see their Section 2.2, Fig. 1, Tables 1 and 2). Briefly, we tested the exchange column procedure by processing aliquots of our pure dissolved in-house Si-isotope standard, a Si solution with a typical Mg-rich silicate matrix, and a Si solution with a high Fe-matrix through the entire column chemistry, and compared the eluted Si to the known value for this standard. The final measured Si-isotopic compositions were not affected by the presence of these other elements. Dissolution of Si in concentrated HCl also showed no associated isotope fractionation. The entire analytical protocol (sample dissolution, cation exchange chemistry, and mass spectrometry) was tested by measuring δ^{30}Si and δ^{29}Si values of available international Si-isotope standards (Reynolds et al., 2007), and SC olivines (Table 1).

2.6. Accuracy of Si-isotope results

Silicon isotope analyses were validated by analyses of several Si-isotope standards (Table 1). The international reference Si-isotope standard is NBS-28, and has, per definition, a δ^{30}Si value of 0.0‰. We used NBS-28 as a primary standard in this study for both the solution and the laser-ablation analyses. Our solution in-house secondary standard has a $\delta^{30}Si_{NBS\text{-}28}$ value of −2.15 ± 0.04 (2se) ‰ based on multiple determinations. We analyzed three Si-isotope samples regarded as standard materials for solution MC-ICPMS analyses: IRMM-018a, Diatomite, and “Big Batch” (Table 1). Their silicon-isotopic compositions were previously reported in an inter-laboratory comparison (Reynolds et al., 2007). We note that Big Batch is known to contain some trace amounts of Mo (van den Boorn et al., 2006), a relic of the molybdate co-precipitation technique used (De La Rocha et al., 1996) to

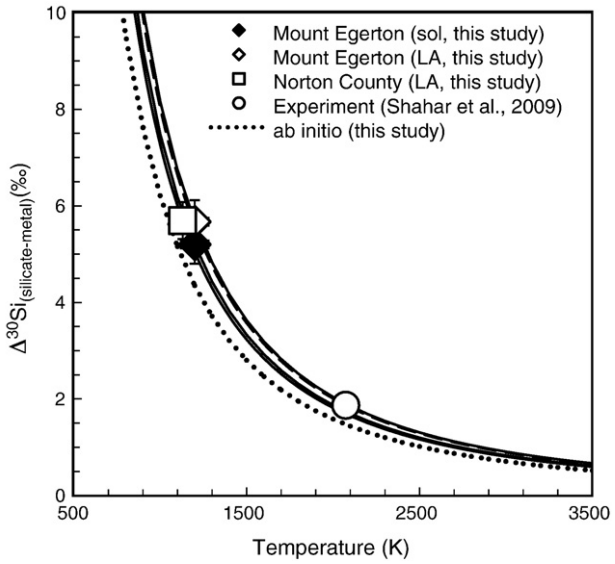

Fig. 1. $\Delta^{30}Si_{silicate-metal}$ vs. temperature (K) plot. The solid lines are $1/T^2$ curves anchored to the averages of the Mount Egerton solution data, the Mount Egerton laser-ablation data, and the Norton County laser-ablation data. Equations for these curves are: $\Delta^{30}Si_{silicate-metal} = (7.49\times10^6)/T^2$, $\Delta^{30}Si_{silicate-metal} = (8.17\times10^6)/T^2$ and $\Delta^{30}Si_{silicate-metal} = (7.27\times10^6)/T^2$ for Mount Egerton solution, Mount Egerton laser ablation, and Norton County, respectively. The dashed curve represents the equation $\Delta^{30}Si_{silicate-metal} = (8.04\times10^6)/T^2$ and is anchored to the experimental datum of Shahar et al. (2009). The dotted curve is the calculated ab initio equilibrium fractionation between forsterite and solid Fe_3Si at low pressures (~10 GPa) corresponding to $\Delta^{30}Si_{silicate-metal} = (-1.6572\times10^{11}/T^4 + 6.3756\times10^6/T^2)$.

prepare the standard, and therefore has somewhat larger uncertainties (Cardinal et al., 2003; Carignan et al., 2004; van den Boorn et al., 2006; Chmeleff et al., 2008). In addition, we analyzed a separate of SC olivine (mantle xenolith), a representative of a material with a more complicated matrix chemistry that other laboratories have analyzed.

Our $\delta^{30}Si$ results for the international Si-isotope standards for solution MC-ICPMS are within <0.1‰ of the average values reported by Reynolds et al. (2007). Our SC olivine $\delta^{30}Si_{NBS-28}$ value of -0.28 ± 0.06‰ compares well to values from other mantle olivines of -0.33 ± 0.03 and -0.3 ± 0.1‰ (Georg et al., 2007, solution MC-ICPMS; Douthitt, 1982, and references therein; SiF_4 dual inlet) (Table 1). Douthitt (1982) reports his values relative to Rose Quartz Standard, but this standard has been found to be identical to NBS-28 (De La Rocha et al., 1997; Georg et al., 2007).

Our in-house standard for laser-ablation MC-ICPMS (San Carlos olivine USNM 136718) has a $\delta^{30}Si_{NBS-28}$ value of -0.32 ± 0.12‰ based on multiple laser-ablation determinations (Table 1).

A comparison of $\delta^{30}Si_{NBS-28}$ values obtained by both solution and laser-ablation MC-ICPMS (Table 1) shows that laser-ablation results of silicates are within ~0.1‰ of the result obtained by solution analysis. The $\delta^{30}Si_{NBS-28}$ values of the metal show a larger offset of 0.6‰ (~2 times the analytical precision) between the laser ablation and the solution technique, presumably due to the very low Si concentrations in metal. This offset is relatively small in comparison to the large fractionations investigated here.

3. Isotope results

Our San Carlos olivine results include 4 different San Carlos materials (Table 1), and two different analytical techniques. $\delta^{30}Si_{NBS-28}$ values range from −0.27 to −0.45‰, averaging -0.33 ± 0.08 (2se) ‰. This result compares well with previously published mantle data. Our $\delta^{30}Si$ results for E chondrites agree well with those analyzed by Fitoussi et al. (2009) and Georg et al. (2007). Our Murchison sample agrees to within <0.1‰ with that of Georg et al. (2007), but shows larger discrepancies with the Fitoussi et al. (2009) and the Molini-Velsko et al. (1986) data. Molini-Velsko et al. (1986) analyzed various components of Murchison, and obtained a 1.0‰ spread in $\delta^{30}Si$ (0.2‰ 1σ analytical precision); the average of -0.7 ± 0.4‰, at face value would indicate that all data are within analytical error. However, excluding a 0.0‰ 'outlier', gives an average value of −0.8‰ with a 1σ of 0.2‰, indicating that these data hint at sample inhomogeneity in Murchison (Table 1).

The $\delta^{30}Si_{NBS-28}$ value of the Mount Egerton enstatite obtained by solution MC-ICPMS is -0.73 ± 0.32 (2se) ‰, and that obtained by laser ablation is -0.88 ± 0.06‰. Laser-ablation analysis of the Norton County enstatite give $\delta^{30}Si_{NBS-28} = -0.93\pm0.10$‰. These values are more negative than those of the two E chondrites Abee and Indarch (-0.61 ± 0.08 and -0.65 ± 0.08‰, respectively). The Si in the metal of these two meteorites has significantly more negative $\delta^{30}Si_{NBS-28}$ values of -5.93 ± 0.16‰ (solution) and -6.55 ± 0.20‰ (laser ablation) for Mount Egerton, and -6.62 ± 0.28‰ (laser ablation) for Norton County (Table 1). The resulting $\Delta^{30}Si_{silicate-metal}$ values are 5.20 ± 0.36‰ (2 se) (solution) and 5.67 ± 0.21‰ (laser ablation) for Mount Egerton, and 5.69 ± 0.30‰ (laser ablation) for Norton County.

These results for silicate–metal Si-isotope fractionation afford the opportunity to place the concept of using Si-isotope fractionation as a monitor of core formation (Eq. (1)) on a firm foundation because it can be used to derive a calibration for the relationship between $\Delta^{30}Si_{silicate-metal}$ and temperature in natural materials.

4. Equilibrium isotope fractionation

4.1. Si silicate–metal fractionation in Mount Egerton and Norton County

The deduced equilibration temperature of 1200 ± 80 K for Mount Egerton and 1130 ± 80 K for Norton County (Section 2.1) yields a calibration for a wide range of temperatures because stable isotope fractionation at high temperatures varies approximately with the inverse square of temperature (Urey, 1947). A $1/T^2$ curve through the Mount Egerton data point obtained by solution MC-ICPMS analyses yields an equilibrium silicon isotope fractionation between Si in metal and Si in silicate of $\Delta^{30}Si_{silicate-metal} = 7.49\times10^6/T^2$. The equivalent using the laser-ablation measurements is $\Delta^{30}Si_{silicate-metal} = 8.17\times10^6/T^2$. The Norton County laser-ablation data yield $\Delta^{30}Si_{silicate-metal} = 7.27\times10^6/T^2$ (Fig. 1). The average equilibrium silicon isotope fractionation between Si in metal and Si in silicate obtained from these natural samples, therefore, is:

$$\Delta^{30}Si_{silicate-metal} = \frac{7.64\times10^6 \pm 0.47(1\sigma)}{T^2}. \quad (2)$$

The uncertainty in calculated silicate–metal $^{30}Si/^{28}Si$ fractionation obtained from Eq. (2) is $\sigma^2_{\Delta^{30}Si} = (-2A/T^3)^2\sigma^2_T + (1/T^2)\sigma^2_A$, where A is the constant numerator on the right hand side of Eq. (2). At 1200 K ± 80 K, the uncertainty in A has negligible impact on the calculated fractionation, while the uncertainty in temperature contributes almost the entire total uncertainty of 0.7‰ (1σ) in $\Delta^{30}Si_{silicate-metal}$. Conversely, application of Eq. (2) to arrive at a temperature results in an uncertainty in that temperature of ±19 K for a measured $\Delta^{30}Si_{silicate-metal}$ value of 6.0 ± 0.2‰.

The reliability of the calibration in Eq. (2) depends in part on the likelihood for resetting of the Si-isotope system with continual cooling. We assess the possibility for Si-isotope closure at a temperature lower than that indicated by Si solubility in metal by examining the self diffusion of Si in silicate and metal. The rate of self diffusion of Si is significantly greater in metal than in silicate. The characteristic diffusion length scale ($\sqrt{D_{Si}t}$, where D_{Si} is the self diffusion coefficient for Si and t is time) for Si diffusion in FeSi is 1 mm at 1200 K for a time period of 1000 years (Riihmäki et al., 2008). For the same temperature and time interval, the characteristic diffusion length scale for olivine (similar to that in pyroxene) is 10^{-3} μm (Dohmen et al., 2002); Si self diffusion is 6 orders of magnitude slower

Table 1
Silicon isotope ratios of international Si-isotope standards, mantle olivines and meteorite samples.

			δ^{29}Si(‰ NBS-28)		δ^{30}Si(‰ NBS-28)	
Standards	Ref.[a]	*n*	Av.	2se	Av.	2se
IRMM-018a	This study, solution	2	−0.79	0.02	−1.55	0.18
	This study, laser	5	−0.97	0.18	−1.65	0.30
	(1)		−0.85	0.01	−1.65	0.11
Diatomite	This study, solution	1	0.630	0.008	1.22	0.18
	(1)		0.64	0.02	1.26	0.02
Big Batch	This study, solution	2	−5.33	0.26	−10.38	0.60[b]
	(1)		−5.35	0.02	−10.48	0.04
Earth mantle olivines						
San Carlos (SC) Harvard	This study, solution	5	−0.15	0.02	−0.28	0.06
SC CEM 1–3	This study, laser	9	−0.18	0.04	−0.27	0.04
SC UCLA	This study, laser	9	−0.28	0.06	−0.45	0.12
SC USNM	This study, laser	12	−0.21	0.06	−0.32	0.12
Cameroon lherzolite	(2)[c]	20	−0.15	0.03	−0.33	0.03
dunite, N.C.	(3)[d]				−0.3	0.1
Meteorites						
Murchison	This study, solution	1	−0.37	0.04	−0.73	0.04
	(2)	33	−0.34	0.03	−0.65	0.03
	(4)[e]		−0.40		−0.94	
	(4)[f]		−0.26		−0.50	
	(4)[g]		0.02		0.00	
	(4)[h]		−0.39		−0.71	
	(4)[i]		−0.40		−0.80	
	(4)[j]		−0.56		−1.11	
	(5)	4	−0.18	0.03	−0.36	0.05
Abee silicate	This study, solution	3	−0.31	0.02	−0.61	0.08
	(2)	11	−0.36	0.01	−0.69	0.03
Indarch silicate	This study, solution	3	−0.33	0.04	−0.65	0.08
	(4)[k]		−0.23		−0.46	
Mount Egerton *enstatite*	This study, solution	5	−0.37	0.16	−0.73	0.32
	This study, laser	37	−0.49	0.04	−0.88	0.06
Mount Egerton *metal*	This study, solution	5	−3.08	0.08	−5.93	0.16
	This study, laser	15	−3.44	0.12	−6.55	0.20
Norton County *enstatite*	This study, laser	30	−0.52	0.06	−0.93	0.10
	(4)		−0.48		−1.03	
Norton County *metal*	This study, laser	4	−3.57	0.14	−6.62	0.28

Uncertainty(2 *standard error*) = 2 × *standard deviation* / $\sqrt{n}$.

[a] References: (1) Reynolds et al. (2007), combination of techniques, (2) Georg et al. (2007), solution MC-ICPMS, (3) Douthitt (1982), SiF_4 by dual inlet mass spectrometry, (4) Molini-Velsko et al. (1986) (SiF_4 by dual inlet mass spectrometry, analytical uncertainty for δ^{30}Si given as 0.2‰ at a 1σ level), (5) Fitoussi et al. (2009), solution MC-ICPMS.

[b] See Section 2.6 for explanation of large uncertainty.

[c] Average of 2 olivines from Cameroon Line spinel lherzolite.

[d] Olivine from a dunite from North Carolina.

[e] Matrix value.

[f] Olivine/pyroxene fraction (3.0<*d*<3.23).

[g] Mostly olivine fraction (3.26<*d*<3.28).

[h] Xenolith clast.

[i] Chondrule.

[j] Bulk meteorite.

[k] Non-magnetic fraction.

in silicate than in metal. Consequently, it is the closure of Si diffusion in silicate that limits the possibility for isotopic exchange with cooling. It is not the classical closure temperature that is important in this context, however, but rather the amount of Si accessible to metal by diffusion in enstatite. Access to only a small fraction of the Si in enstatite by diffusion could, in principle, substantially affect the δ^{30}Si value of the Si in metal. The likelihood for such an exchange can be assessed in terms of the temperature-dependent diffusivity of Si in enstatite. For a 1 mm diameter crystal of enstatite, the width of the outer annulus necessary to provide sufficient Si to exchange with metal by self diffusion is 3 μm. This is 3 orders of magnitude larger than the characteristic diffusion length scale of 10^{-3} μm at 1200 K and 1000 years cited above. In order to reach the necessary amount of Si for isotope exchange with metal at 1200 K, 500 million years would be required, and longer times at lower temperatures. We conclude that it is unlikely that significant Si-isotope exchange occurred between enstatite and metal at temperatures lower than that recorded by the solubility of Si in metal.

The veracity of the relationship in Eq. (2) can be assessed by comparing it to the fractionation predicted by theory and experiment.

4.2. Experimentally-determined equilibrium Si-isotope fractionation

A recent experimental study of Si-isotope fractionation between silicate melt and Si-bearing Fe metal suggests a 1.9‰ fractionation at 2073 K, 1 GPa, and an f_{O_2} of approximately $\Delta IW = -4$ ($\Delta IW = \log(f_{O_2}) - \log(f_{O_2})_{IW}$, where IW represents the fugacity of oxygen defined by the reaction Fe (Iron) + 1/2 O_2 = FeO (Wüstite)) (Shahar et al., 2009). This experimental datum yields (Fig. 1)

$$\Delta^{30}Si_{\text{silicate-metal}} = \frac{8.04 \times 10^6}{T^2}, \quad (3)$$

Table 2
Parameters used for isopleths diagrams.

Parameters for $\log\left(\frac{x_{Si}^{metal}}{x_{SiO_2}^{silicate}}\right)$		
a	2.97	
b	−21,800	
c	−11	
d	−0.24	
nbo/t	2.1	
γ_{Si}° metal	0.007	
γ_{Si}° metal reference T° (K)	2273	
γ_{Fe}° metal	0.8	
γ_{Fe}° metal reference T° (K)	2273	
$\gamma_{FeO}^{silicate}$	4	
Magma ocean adiabat		
C_p	1000	J/(kg K)
ρ	4000	kg/m^3
α	5×10^{-5}	K^{-1}
T base of magma ocean (T_{base})	3116	K
P base of magma ocean (P_{base})	40	GPa
Masses		
Mass Earth	5.9736×10^{24}	kg
Mass fraction core	0.3	
Mass core	1.7921×10^{24}	kg
Mass BSE	4.1815×10^{24}	kg
Mass fraction Si BSE	0.21	
Mass Si BSE	8.7812×10^{23}	kg
Earth composition (present-day)		
Mass fraction SiO_2	0.55	
Mass fraction MgO	0.37	
Mass fraction FeO	0.08	
$x_{FeO}^{silicate}/x_{Fe}^{metal}$ (molar)	0.063	
$\log fO_2 - \log fO_{2(IW)}$	−0.997	

and compares favorably with the result obtained from the two aubrite meteorites (c.f. Eq. (2)).

4.3. Theoretical equilibrium Si-isotope fractionation predictions

Equilibrium between Earth's growing core and silicate mantle almost certainly occurred at pressures greater than those attending equilibration of the Mount Egerton and Norton County meteorites, or those represented by the experiments (Shahar et al., 2009) (e.g., 40 GPa, Zerr et al., 1998; Wood, 2008). However, silicate–metal Si-isotope fractionation factors based on ab initio calculations indicate that pressure has little effect on $\Delta^{30}Si_{silicate-metal}$ (Shahar et al., 2009). Therefore, to a first approximation, an extension of the low-pressure equilibrium fractionation relationship to high-pressure settings is valid (the pressure effect is <0.1‰; see Fig. 5 in Shahar et al., 2009). A theoretical prediction for $^{30}Si/^{28}Si$ fractionation between forsterite and Fe_3Si as a function of temperature (Fig. 1) gives

$$\Delta^{30}Si_{silicate-metal} \sim 10^3 \ln\left(\alpha_{Fo-Fe_3Si}^{30/28}\right) = \frac{6.38\times10^6}{T^2} - \frac{1.66\times10^{11}}{T^4} \quad (4)$$

where $\alpha_{Fo-Fe_3Si}^{30/28}$ is the equilibrium fractionation factor defined as $(^{30}Si/^{28}Si)_{forsterite}/(^{30}Si/^{28}Si)_{Fe_3Si}$.

4.4. Comparing Si-isotope fractionation between silicate and metal from meteorites, experiments, and theory

The average temperature dependence of $\Delta^{30}Si_{silicate-metal}$ derived from meteorites (Eq. (2)) is indistinguishable from that obtained from experiments (Shahar et al., 2009) (Eq. (3)), while both relationships indicate slightly higher temperatures and larger $\Delta^{30}Si_{silicate-metal}$ values than those predicted from lattice dynamic calculations (Eq. (4), Fig. 1). The agreement between Eqs. (2) and (3) (within uncertainties), and the rough agreement of both measured calibrations with the theoretical prediction (Eq. (4)), is important because each calibration is based on silicate and metal phases of different compositions. We conclude that the relationship between $\Delta^{30}Si_{silicate-metal}$ and temperature is known to the precision described above, regardless of the exact compositions of the silicate and metal phases.

5. Si in Earth's core

5.1. Isotopic constraints on the concentration of Si in the core

The essential parameter for extrapolating our isotope data to conditions relevant to Earth's core formation using Eq. (1) is temperature, because pressure has little effect on $\Delta^{30}Si_{silicate-metal}$ (Shahar et al., 2009), and because $\Delta^{30}Si_{silicate-metal}$ is independent of f_{O_2}. The latter statement may seem cavalier at first, but we emphasize that f_{O_2} controls the concentration of Si in metal, but not the nature of the bonding of Si in metal; and it is the bond stiffness, and not concentration, that controls fractionation. Estimates for temperatures of core formation in Earth vary within limits. Multi-stage core accretion is the most likely model (Javoy, 1995; Gessmann et al., 2001; Wade and Wood, 2005; Corgne et al., 2008; Frost et al., 2008; Wood, 2008). One of these continuous metal segregation models satisfies all constraints from chemical partitioning between core and BSE with an average temperature of ~3000 K (Wade and Wood, 2005).

Recent estimates for $\delta^{30}Si_{BSE}$ and $\delta^{30}Si_{chondrite}$ have produced a range of values for $\Delta^{30}Si_{BSE\text{-}chondrite}$ from 0.08 to 0.20‰ (Georg et al., 2007; Armytage et al., 2009; Fitoussi et al., 2009). We obtained $\delta^{30}Si$ values for SC olivine (-0.33 ± 0.08 2se‰), and those of silicate phases of several chondrites (-0.73 ± 0.12‰) (Table 1), suggesting an average $\Delta^{30}Si_{BSE\text{-}chondrite}$ value of 0.4 ± 0.14‰ (Fig. 2). If only enstatite chondrites are used for $\Delta^{30}Si_{BSE\text{-}chondrite}$ calculations, we obtain a $\Delta^{30}Si_{BSE\text{-}chondrite}$ value of -0.30 ± 0.09‰ that compares well with the same BSE-enstatite chondrite fractionations of Georg et al. (2007) and Fitoussi et al. (2009) (-0.31 ± 0.06 and -0.27 ± 0.04‰, respectively), and that is only slightly outside their $\Delta^{30}Si_{BSE\text{-}chondrite}$ values obtained when using ordinary chondrites (-0.19 ± 0.07 and -0.14 ± 0.03‰, respectively) (all 1σ). Variability in $\Delta^{30}Si_{BSE\text{-}chondrite}$ appears to be primarily in the $\delta^{30}Si$ value of carbonaceous chondrites.

In light of the uncertainty and range in $\Delta^{30}Si_{BSE\text{-}chondrite}$, we show here the sensitivity of the calculated mass of Si in Earth's core to this parameter (Fig. 3). For the range of $\Delta^{30}Si_{BSE\text{-}chondrite}$ values of between ~0.1 and 0.3‰ published previously (Georg et al., 2007; Armytage et al., 2009; Fitoussi et al., 2009) and from this study, the calibration in Eq. (2), and a core formation temperature of ~3000 K (Wade and Wood, 2005), the mass of Si in the core is between ~6 and ~25 wt.% (Fig. 3). The low end of this range is consistent with estimates based on geophysical and cosmochemical considerations (McDonough and Sun, 1995; McDonough, 2003; Badro et al., 2007). We note that a $\Delta^{30}Si_{BSE\text{-}chondrite}$ value of 0.14‰ corresponds to a chondritic Mg/Si ratio of 0.904 (McDonough and Sun, 1995) at ~3000 K for bulk Earth, and would be compatible with existing isotope data. We point out that the derivatives of the curves in Fig. 3 decrease substantially where $\Delta^{30}Si_{BSE\text{-}chondrite}$ values exceed 0.2‰, resulting in very high sensitivities of the resulting wt.% Si to $\Delta^{30}Si_{BSE\text{-}chondrite}$. Even small uncertainties in $\Delta^{30}Si_{BSE\text{-}chondrite}$ at values beyond 0.2‰ lead to large errors in wt.% Si at high temperature (Fig. 3).

5.2. Isotopic constraints on oxidation state during metal segregation

Based on elemental partitioning studies, f_{O_2} during Earth's core formation is believed to have increased during continuous multi-stage accretionary processes, with initial f_{O_2} possibly as low as $\Delta IW = -6$

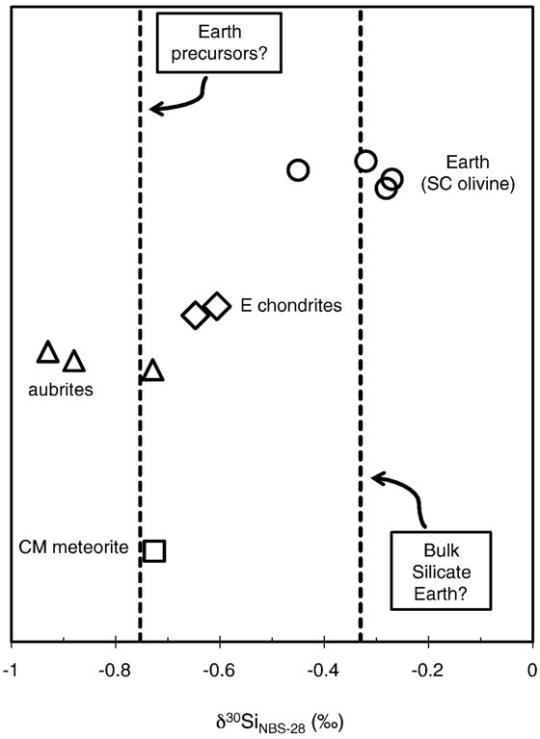

Fig. 2. Si-isotope ratios of meteorites and terrestrial San Carlos olivine analyzed in this study. The two dashed lines represent the average of all meteorites and the average SC olivines from this study.

(Javoy, 1995; Gessmann et al., 2001; Wade and Wood, 2005; Corgne et al., 2008; Frost et al., 2008; Wood, 2008; Cottrell et al., 2009). This inferred oxidation level is consistent with the estimated prevailing f_{O_2} of near ΔIW − 6 during formation of enstatite meteorites (Berthet et al., 2009). Establishment of the relationship between $\Delta^{30}Si_{silicate-metal}$ and equilibration temperature provides further constraints on f_{O_2} during core formation. For this purpose, we used the thermodynamics of Si

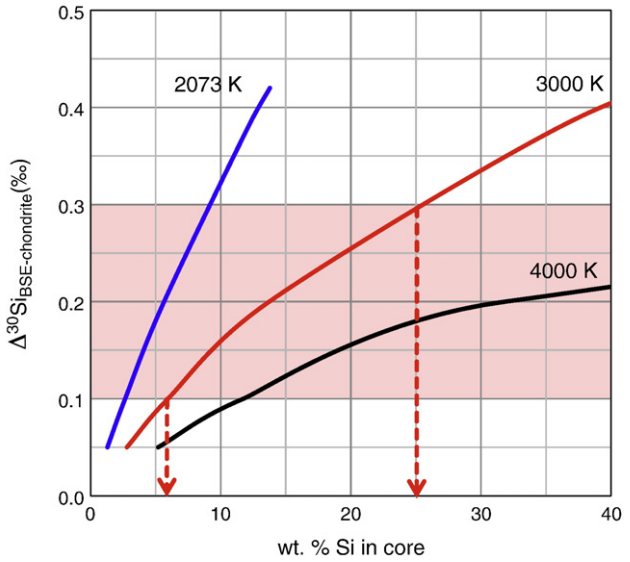

Fig. 3. $\Delta^{30}Si_{BSE\text{-}chondrite}$ plotted against calculated wt.% Si in the metal core using Eq. (1) and the calibration for $\Delta^{30}Si_{silicate-metal}$ provided by the meteorite measurements (Eq. (2)). At the suggested temperature of Earth's core equilibration of ~3000 K (Wood, 2008), the range of reported $\Delta^{30}Si_{BSE\text{-}chondrite}$ of ~0.1 to 0.3‰ (shaded area; Georg et al., 2007; Armytage et al., 2009; Fitoussi et al., 2009; this study) suggests between ~6 and 25 wt.% Si in the core (arrows).

solubility in metal established experimentally (Corgne et al., 2008), temperatures and pressures corresponding to an isoentropic adiabat through Earth's magma ocean, and the Si-isotope mass balance (Eq. (1)) to calculate both the wt.% of Si in the core and $\Delta^{30}Si_{BSE\text{-}chondrite}$ as functions of ΔIW and $P(T)$ along the magma ocean adiabat (Figs. 4 and 5).

In order to relate the equilibrium concentrations of Si in metal and in silicate to observed Si-isotope ratios, we link the isotope mass balance (Eq. (1)) to the thermodynamics of Si solubility in the core by noting that the fraction of Earth's Si in the core can be converted to the mole fraction of Si in the core:

$$x_{Si}^{core} = \frac{f_{Si,core}}{1-f_{Si,core}} \frac{M_{BSE}}{M_{core}} \frac{MW_{core}}{MW_{Si}} \quad (5)$$

where M_i is the mass of component i, MW_i is the molecular weight of component i, and x_{Si}^{core} is the mole fraction of Si in the metal core. MW_{core} is calculated assuming the core is composed only of Fe and Si.

Although uncertain, ~40 GPa has been suggested as average pressure for the base of Earth's magma ocean (Wood, 2008). The solidus (~liquidus at these pressures) for mantle rocks at 40 GPa is ~3100 K (Zerr et al., 1998; Wood, 2008). We adopted these conditions for our calculations. Under the assumption that the magma ocean was well mixed, we used an isoentropic adiabat to define the relationship between P and T as described by Solomatov (2000). The expression for the adiabat is

$$T = \frac{T_{base}}{1 + \frac{\alpha}{\rho C_p}(P_{base} - P)}, \quad (6)$$

where $\alpha = 5 \times 10^{-5}\,K^{-1}$ is the thermal expansivity for the magma ocean, $\rho = 4 \times 10^3\,kg\,m^{-3}$ is the density of the magma, and $C_p = 1 \times 10^3\,J kg^{-1}\,K^{-1}$ is the isobaric heat capacity (Solomatov, 2000). Our adiabatic P-axis on the contour diagrams presented here corresponds to varying P and T as prescribed by Eq. (6).

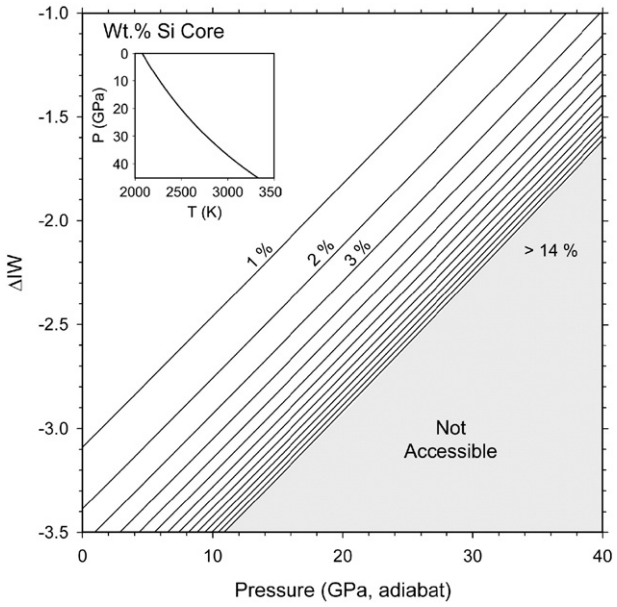

Fig. 4. Isopleths for the mass of Si in metal (wt.%) plotted as a function of ΔIW and $P(T)$ (adiabatic P–T-relationship shown in inset). Isopleths for wt.% Si in the core (in 1 wt.% intervals) are shown. Eq. (2) was used for the metal–silicate isotope fractionation calibration. The ΔIW–$P(T)$ area above ~14 wt.% Si has been labeled "not accessible" as such high concentrations of Si in the core are not plausible. If it was assumed that the current oxidation level of the lower mantle of ΔIW − 1.0 also prevailed during core formation at the bottom of the magma ocean (40 GPa), the amount of Si in the core would be limited to no more than 3 wt.%.

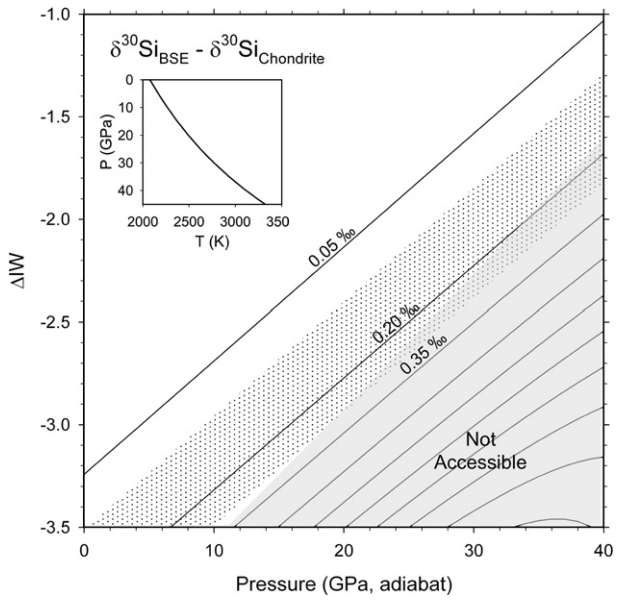

Fig. 5. Calculated isopleths for $\Delta^{30}Si_{BSE\text{-}chondrite}$ (‰) plotted as a function of ΔIW and $P(T)$ (adiabatic P–T-relationship shown in inset). Isopleths are shown in 0.15‰ intervals. Eq. (2) was used for the metal–silicate isotope fractionation calibration. The grey "not accessible" area (based on limits of plausible wt.% Si in metal from Fig. 4) constrains plausible $\Delta^{30}Si_{BSE\text{-}chondrite}$ values to no greater than ~0.20‰ at 40 GPa, the maximum pressure inferred for the base of the magma ocean. At that pressure, the most likely range of $\Delta^{30}Si_{BSE\text{-}chondrite}$ values (0.1 to 0.3‰, stippled area) corresponds to ΔIW values of ~−1.3 to −1.7. Lower magma ocean pressures would suggest lower ΔIW values.

In order to quantify the relationships between the solubility of Si in metal, f_{O_2}, P, T, and $\Delta^{30}Si_{silicate\text{–}metal}$, recent thermodynamic data (Corgne et al., 2008) at temperatures and pressures relevant to core formation are used. The relationship between Si solubility in molten Fe metal and f_{O_2} was obtained by combining two equilibria:

$$FeO_{silicate\ liq} \rightleftharpoons Fe_{metal\ liq} + \frac{1}{2}O_2 \tag{7}$$

and

$$(SiO_2)_{silicate\ liq} + 2Fe_{metal\ liq} \rightleftharpoons 2FeO_{silicate\ liq} + Si_{metal}. \tag{8}$$

The equilibrium constants for the two reactions are

$$k_{eq,7} = \frac{a_{Fe}^{metal}\left(f_{O_2}\right)^{1/2}}{a_{FeO}^{silicate}} \tag{9}$$

and

$$k_{eq,8} = \frac{\left(a_{FeO}^{silicate}\right)^2 a_{Si}^{metal}}{\left(a_{Fe}^{metal}\right)^2 a_{SiO_2}^{silicate}}. \tag{10}$$

The first equilibrium constant can be expanded to obtain an explicit expression for f_{O_2}. For this purpose we concentrate on the differences from f_{O_2} prescribed by the IW buffer. We start with

$$\frac{1}{2}\log\left(f_{O_2}\right) = -\frac{\Delta G_{rxn}^{o}}{2.303RT} + \log\left(\frac{a_{FeO}^{silicate}}{a_{Fe}^{metal}}\right) \tag{11}$$

and recognize that changes in $\log(f_{O_2})$, with respect to changes in the activity ratio on the right hand side of Eq. (11), involve the derivative only; the constant containing the reaction free energy change at standard state and fixed T vanishes in the derivative, and we are left with

$$\frac{d\log\left(f_{O_2}\right)}{d\log\left(\frac{a_{FeO}^{silicate}}{a_{Fe}^{metal}}\right)} = 2. \tag{12}$$

We are interested in deviations in $\log(f_{O_2})$ from the IW buffer. Because the IW buffer is composed of the pure Fe and FeO phases, Eq. (12) becomes

$$\Delta IW = \log\left(f_{O_2}\right) - \log\left(f_{O_2}\right)_{IW} = 2\log\left(\frac{a_{FeO}^{silicate}}{a_{Fe}^{metal}}\right) - 0 \tag{13}$$

which is rewritten as

$$\Delta IW = 2\log\left(\frac{x_{FeO}^{silicate}}{x_{Fe}^{metal}}\right) + 2\log\left(\frac{\gamma_{FeO}^{silicate}}{\gamma_{Fe}^{metal}}\right) \tag{14}$$

where x_i represents the mole fraction of species i in the specified phase, and γ_i the corresponding activity coefficient. The values for γ_{Fe}^{metal} and $\gamma_{FeO}^{silicate}$ in the molten phases are nearly constant at 0.8 and 3.0 ± 0.1, respectively (Corgne et al., 2008, and references therein). We apply a small temperature dependence for the former, nonetheless (see below).

The equilibrium constant for the Si–Fe exchange reaction between molten silicate and molten Fe-rich metal (Eq. (10)) can be expanded in terms of mole fractions, activity coefficients, and thermodynamic constants. Regressions of experimentally-determined values for $k_{eq,8}$, excluding the activity coefficients for the silicate melt (assuming their ratio to be constant) (Wade and Wood, 2005; Corgne et al., 2008), yields

$$\log k_{eq,8} - \log\left(\frac{\left(\gamma_{FeO}^{silicate}\right)^2}{\gamma_{SiO_2}^{silicate}}\right) = a + \frac{b}{T} + \frac{cP}{T} + d\frac{nbo}{t} \tag{15}$$

where nbo/t is the ratio of non-bridging oxygens to tetrahedrally-coordinated cations in silicate melt. Fit parameters a, b, c and d, obtained from regressing experimental data (Corgne et al., 2008) are listed in Table 7 of that work. Parameters a, b, and c can be regarded as apparent values for $-\Delta\hat{S}^{\circ}_{rxn}/(R\ \ln(10)) + \log((\gamma_{FeO}^{silicate})^2/\gamma_{SiO_2}^{silicate})$, $\Delta\hat{H}^{\circ}_{rxn}/(R\ln(10))$, and $\Delta\hat{V}^{\circ}_{rxn}/(R\ln(10))$, respectively, where R is the gas constant and the other symbols are the usual changes in molar thermodynamic parameters for reaction (8) based on standard states defined by the pure phases. For the silicate melts of interest here, nbo/t is between 2.7 and 1.8. We used the intermediate value of 2.1 suggested by the authors, but the precise value within the range cited has negligible influence on our results. Eq. (15) is rearranged (Corgne et al., 2008) to obtain

$$\log\left(\frac{x_{Si}^{metal}}{x_{SiO_2}^{silicate}}\right) = a + \frac{b}{T} + \frac{cP}{T} + d\frac{nbo}{t} - 2\log\left(\frac{x_{FeO}^{silicate}}{x_{Fe}^{metal}}\right) - \log\left(\frac{\gamma_{Si}^{metal}}{\left(\gamma_{Fe}^{metal}\right)^2}\right). \tag{16}$$

For our purposes we reintroduce $\log(f_{O_2})$ explicitly into Eq. (16) by substituting Eq. (14) for the 4th term on the right hand side to obtain

$$\log\left(\frac{x_{Si}^{metal}}{x_{SiO^2}^{silicate}}\right) = a + \frac{b}{T} + \frac{cP}{T} + d\frac{nbo}{t} - \Delta IW + 2\log\left(\frac{\gamma_{FeO}^{silicate}}{\gamma_{Fe}^{metal}}\right) - \log\left(\frac{\gamma_{Si}^{metal}}{\left(\gamma_{Fe}^{metal}\right)^2}\right). \tag{17}$$

Solutions to Eq. (17) were used to create the isopleths in Figs. 4 and 5. We reiterate that the link between isotope fractionation and Si solubility arises because of the link between Eqs. (1) and (17) afforded by recasting the fraction of Earth's silicon that resides in the core, $f_{\text{Si-core}}$, to the mole fraction of Si in the core, $x_{\text{Si}}^{\text{core}}$ (Eq. (5)). In this formulation, $\gamma_{\text{FeO}}^{\text{silicate}}$ must be known while it is absent in the formulation used by Corgne et al. (2008) (i.e., Eq. (16)). For internal consistency, we calibrated $\gamma_{\text{FeO}}^{\text{silicate}}$ by comparing our calculated log $(x_{\text{Si}}^{\text{metal}}/x_{\text{SiO}_2}^{\text{silicate}})$from Eq. (17) with the experiments of Corgne et al. (2008). We find that the experimental data are reproduced (e.g., Fig. 3 in Corgne et al., 2008) if $\gamma_{\text{FeO}}^{\text{silicate}} = 4$. For the two activity coefficients applicable to molten alloy in Eq. (17), we adopted the following temperature dependence (Corgne et al., 2008):

$$\ln \gamma_i^{\circ}(T) = \frac{T^{\circ}}{T} \ln \gamma_i^{\circ}(T^{\circ}) \tag{18}$$

where γ_i° and T° refer to the activity coefficient and temperature of a reference state corresponding to an infinitely dilute component i at the prescribed reference temperature. The reference values were taken from Table 6 of Corgne et al. (2008). The parameters used in our thermodynamic calculations are listed in Table 2.

Uncertainties in the thermodynamic calculations and the calibration of isotope fractionation impart an uncertainty to these estimates of order 0.2 in ΔIW with one exception, and that is the uncertainty in volume changes associated with Si dissolution in metal. The full range of estimated values for this pressure effect on Si solubility in metal corresponds to a 0.5 log unit systematic uncertainty in the calculated ΔIW values for the isopleths in Figs. 4 and 5.

As a check on the consistency of the different approaches, namely the isotope fractionation equation (Eq. (2)) and the Si solubility thermodynamic calculations, we applied Eq. (17) to the Mount Egerton phase compositions. The 1200 K obtained by applying the chemistry data for Mount Egerton to Wasson et al.'s (1994) calibration, approaches, but does not exceed, the solidus for enstatite chondrites (1273 K) (McCoy et al., 1999). We are, therefore, in effect applying a metastable extension of the supersolidus thermodynamics to the subsolidus where the derived temperatures are at or below the solidus. Using the thermodynamic expressions described above, we obtain the observed Si and Fe concentrations in metal and silicate in Mount Egerton when using 1274 K and IW − 8. This value for equilibration temperature is within error of that obtained from the Wasson calibration at similarly low f_{O_2} (<IW − 6); therefore the temperature estimate for Mount Egerton is considered robust with respect to varying activity models and phase changes from solid to liquid.

Based on Eqs. (1), (5), and (17), we find that the reported $\Delta^{30}\text{Si}_{\text{BSE-chondrite}}$ values (Georg et al., 2007; Armytage et al., 2009; Fitoussi et al., 2009; this study) require that during Earth's core formation, f_{O_2} at the base of the magma ocean (at pressures ranging from 25 to 40 GPa) must have been between ΔIW = −2.6 and −1.3 (Fig. 5). The f_{O_2} of the mantle in equilibrium with the core today is ΔIW = −1 based on the FeO concentration of mantle rocks when non-ideal mixing in the silicate and metal phases is included, as in our calculations. ΔIW = −2 is a commonly cited value for current core–mantle boundary conditions that is, however, only obtained for ideal mixing where activity coefficients for Fe and FeO in metal and silicate are assumed to be unity (Corgne et al., 2008). If our calculated present-day lower mantle f_{O_2} of ΔIW = −1 was also characteristic of the base of the magma ocean at the estimated maximum pressure of ~40 GPa during metal segregation, the amount of Si in the core should be at a maximum 3 wt.% (Fig. 4). This would, in turn, necessitate that the $\Delta^{30}\text{Si}_{\text{BSE-chondrite}}$ value be no greater than ~0.05‰ (Fig. 5). The presence of a measurable $\Delta^{30}\text{Si}_{\text{BSE-chondrite}}$ value of at least 0.1‰ and possibly as large as 0.3‰, however, therefore requires that f_{O_2} in the lower mantle increased between the initiation of core formation and the present day by at least 0.5 log units (Fig. 5).

6. Conclusions

The large fractionation of Si isotopes between silicate and metal in the Mount Egerton and Norton County meteorites shows that silicon isotope ratios can be used as indicators of the conditions attending Earth's core formation. Our measurements of $\Delta^{30}\text{Si}_{\text{silicate–metal}}$ values have been made in meteorites that share many characteristics with those inferred for the rocks from which the Earth formed. Establishment of the relationship between $^{30}\text{Si}/^{28}\text{Si}$ fractionation, pressure, temperature, and Si solubility in the core provides an observable constraint, the $\Delta^{30}\text{Si}_{\text{BSE-chondrite}}$ parameter, that links f_{O_2} and Si content of the core if Earth has a chondritic bulk $\delta^{30}\text{Si}$ composition. The results suggest at least 6 wt.% Si in the core by virtue of equilibration at $f_{O_2} \sim 1$ or 2 orders of magnitude lower than that in the present-day lower mantle.

Acknowledgements

This work was supported by grants from the National Science Foundation (NSF EAR-0711411, EDY) and the NASA Cosmochemistry program (EDY). We thank Anat Shahar and Klaus Keil for valuable discussions during the course of this study. We thank Carl Agee (UNM) for providing the Norton County samples.

References

Armytage, R.M.G., Georg, R.B., Halliday, A.N., 2009. The non-chondritic silicon isotope composition of the bulk silicate Earth. 40th Lunar and Planetary Science Conference, Houston, TX, p. 1167.

Badro, J., Fiquet, G., Guyot, F., Gregoryanz, E., Occelli, F., Antonangeli, D., d'Astuto, M., 2007. Effect of light elements on the sound velocities in solid iron: implications for the composition of Earth's core. Earth Planet. Sci. Lett. 254, 233–238.

Bauer, O., Deiss, E., 1915. The Sampling and Chemical Analysis of Iron and Steel. McGraw Hill, London.

Berthet, S., Malavergne, V., Righter, K., 2009. Melting of the Indarch meteorite (EH4 chondrite) at 1 GPa and variable oxygen fugacity: implications for early planetary differentiation processes. Geochim. Cosmochim. Acta 73, 6402–6420.

Birch, F., 1964. Elasticity and constitution of the Earth's interior. J. Geophys. Res. 69, 4377–4388.

Cardinal, D., Alleman, L.Y., de Jong, J., Ziegler, K., André, L., 2003. Isotopic composition of silicon measured by multicollector plasma source mass spectrometry in dry plasma mode. J. Anal. At. Spectrom. 18.

Carignan, J., Cardinal, D., Eisenhauer, A., Galy, A., Rehkämper, M., Wombacher, F., Vigier, N., 2004. A reflection on Mg, Cd, Ca, Li and Si isotopic measurements and related reference materials. Geostand. Geoanal. Res. 28, 139–148.

Casanova, I., McCoy, T.J., Keil, K., 1993a. Metal-rich meteorites from the aubrite parent body. Lunar and Planetary Science Conference XXIV, Lunar and Planetary Institute, Houston, TX, p. 259C.

Casanova, I., Keil, K., Newsom, H.E., 1993b. Composition of metal in aubrites: constraints on core formation. Geochim. Cosmochim. Acta 57, 675–682.

Chmeleff, J., Horn, I., Steinhoefel, G., von Blanckenburg, F., 2008. In situ determination of precise stable Si isotope ratios by UV-femtosecond laser ablation high-resolution multi-collector ICP-MS. Chem. Geol. 249, 155–166.

Corgne, A., Keshav, S., Wood, B.J., McDonough, W.F., Fei, Y., 2008. Metal–silicate partitioning and constraints on core composition and oxygen fugacity during Earth accretion. Geochim. Cosmochim. Acta 72, 574–589.

Cottrell, E., Walter, M.J., Walker, D., 2009. Metal–silicate partitioning of tungsten at high pressure and temperature: implications for equilibrium core formation in Earth. Earth Planet. Sci. Lett. 281, 275–287.

De La Rocha, C.L., Brzezinski, M.A., DeNiro, M.J., 1996. Purification, recovery, and laser-driven fluorination of silicon from dissolved and particulate silica for the measurement of natural stable isotope abundances. Anal. Chem. 68, 3746–3750.

De La Rocha, C.L., Brzezinski, M.A., DeNiro, M.J., 1997. Fractionation of silicon isotopes by marine diatoms during biogenic silica formation. Geochim. Cosmochim. Acta 61, 5051–5056.

Dohmen, R., Chakraborty, S., Becker, H.-W., 2002. Si and O diffusion in olivine and implications for characterizing plastic flow in the mantle. Geophys. Res. Lett. 29, 2030–2034.

Douthitt, C.B., 1982. The geochemistry of the stable isotopes of silicon. Geochim. Cosmochim. Acta 46, 1449–1458.

Fitoussi, C., Bourdon, B., Kleine, T., Oberli, F., Reynolds, B.C., 2009. Si isotope systematics of meteorites and terrestrial peridotites: implications for Mg/Si fractionation in the solar nebula and for Si in the Earth's core. Earth Planet. Sci. Lett. 287, 77–85.

Frost, D.J., Mann, U., Asahar, Y., Rubie, D.C., 2008. The redox state of the mantle during and just after core formation. Philos. Trans. R. Soc. A 366, 4315–4337.
Georg, R.B., Reynolds, B.C., Frank, M., Halliday, A.N., 2006. New sample preparation techniques for the determination of Si isotopic composition using MC-ICPMS. Chem. Geol. 235, 95–104.
Georg, R.B., Halliday, A.N., Schauble, E.A., 2007. Silicon in Earth's core. Nature 447, 1102–1106.
Gessmann, C.K., Wood, B.J., Rubie, D.C., Kilburn, M.R., 2001. Solubility of silicon in liquid metal at high pressure: implications for the composition of the Earth's core. Earth Planet. Sci. Lett. 184, 367–376.
Herndon, J.M., 1996. Substructure of the inner core of the Earth. Proc. Natl. Acad. Sci. U.S.A. 93, 646–648.
Humayun, M., Keil, K., Bischoff, A., 2009. Siderophile elements in metal from Northwest Africa 2526, and enstatite chondrite partial melt residue. 40th Lunar and Planetary Science Conference, Houston, TX, p. 1744.
Javoy, M., 1995. The integral enstatite chondrite model of the earth. Geophys. Res. Lett. 22, 2219–2222.
Keil, K., 1968. Mineralogical and chemical relationships among enstatite chondrites. J. Geophys. Res. 73, 6945–6976.
Larimer, J.W., 1968. Experimental studies on the system Fe–MgO–SiO_2–O_2 and their bearing on the petrology on chondritic meteorites. Geochim. Cosmochim. Acta 32, 1187–1207.
Malavergne, V., Siebert, J., Guyot, F., Gautron, L., Combes, R., Hammouda, T., Borensztajn, S., Frost, D., Martinez, I., 2004. Si in the core? New high-pressure and high-temperature experimental data. Geochim. Cosmochim. Acta 68, 4201–4211.
Mann, U., 2007. Physical and Chemical Constraints on Core–Mantle Differentiation in Terrestrial Planets. Universität Bayreuth.
Mayeda, T.K., Clayton, R.N., 1980. Oxygen isotopic compositions of aubrites and some unique meteorites. LPSC XI, pp. 1145–1151.
McCall, G.J.H., 1965. A meteorite of unique type from Western Australia: the Mount Egerton stony-iron. Mineral. Mag. 35, 241–249.
McCoy, T.J., Dickinson, T.L., Lofgren, G.E., 1999. Partial melting of the Indarch (EH4) meteorite: a textural, chemical, and phase relations view of melting and melt migration. Meteorit. Planet. Sci. 34, 735–746.
McDonough, W.F., 2003. Compositional model for the Earth's core. In: Carlson, R.W. (Ed.), The Mantle and Core. Treatise on Geochemistry, 2. Elsevier-Pergamon, Oxford, pp. 547–568.
McDonough, W.F., Sun, S.-s., 1995. The composition of the Earth. Chem. Geol. 120, 223–253.
Molini-Velsko, C., Mayeda, T.K., Clayton, R.N., 1986. Isotopic composition of silicon in meteorites. Geochim. Cosmochim. Acta 50, 2719–2726.
Newton, J., Franchi, I.A., Pillinger, C.T., 2000. The oxygen-isotopic record in enstatite meteorites. Meteorit. Planet. Sci. 35, 689–698.
Okada, A., Keil, K., Taylor, J., Newsom, H., 1988. Igneous history of the aubrite parent asteroid—evidence from the Norton County enstatite achondrite. Meteoritics 23, 59–74.
Reynolds, B.C., Aggarwal, J., Andre, L., Baxter, D., Beucher, C., Brzezinski, M.A., Engstrom, E., Georg, R.B., Land, M., Leng, M.J., Opfergelt, S., Rodushkin, I., Sloane, H.J., van den Boorn, S.H.J.M., Vroon, P.Z., Cardinal, D., 2007. An inter-laboratory comparison of Si isotope reference materials. J. Anal. At. Spectrom. 22, 561–568.
Riihmäki, I., Virtanen, A., Pusa, P., Salamon, M., Mehrer, H., Räisänen, J., 2008. Si self-diffusion in cubic B20-structured FeSi. Europhys. Lett. 82, 66005.
Ringwood, A.E., 1959. On the chemical evolution and densities of the planets. Geochem. Cosmochim. Acta 15, 257–283.
Ringwood, A.E., 1961. Silicon in the metal phase of enstatite chondrites and some geochemical implications. Geochim. Cosmochim. Acta 25, 1–13.
Rubin, A.E., Keil, K., 1983. Mineralogy and petrology of the Abee enstatite chondrite breccia and its dark inclusions. Earth Planet. Sci. Lett. 62, 118–131.
Rubin, A.E., Scott, E.R.D., 1997. Abee and related EH chondrite impact-melt breccias. Geochim. Cosmochim. Acta 61, 425–435.
Schauble, E.A., 2004. Applying stable isotope fractionation theory to new systems. In: Johnson, C.M., Beard, B., Albarede, F. (Eds.), Geochemistry of Non-traditional Stable Isotopes. Reviews in Mineralogy & Geochemistry, 55. Mineralogical Society of America, pp. 65–111.
Shahar, A., Ziegler, K., Young, E.D., Ricolleau, A., Schauble, E.A., Fei, Y., 2009. Experimentally determined Si isotope fractionation between silicate and Fe metal and implications for Earth's core formation. Earth Planet. Sci. Lett. 288, 228–234.
Solomatov, V.S., 2000. Fluid dynamics of a terrestrial magma ocean. In: Canup, R.M., Righter, K. (Eds.), Origin of the Earth and Moon. University of Arizona Press, Tucson, pp. 323–338.
Urey, H.C., 1947. The thermodynamic properties of isotopic substances. J. Chem. Soc. 562–581.
van den Boorn, A.H.J.M., Vroon, P.Z., van Belle, C.C., van der Wagt, B., Schwieters, J., van Bergen, M.J., 2006. Determination of silicon isotope ratios in silicate materials by high-resolution MC-ICP-MS using a sodium hydroxide sample digestion method. J. Anal. At. Spectrom. 21, 734–742.
Wade, J., Wood, B.J., 2005. Core formation and the oxidation state of the Earth. Earth Planet. Sci. Lett. 236, 78–95.
Wai, C.M., 1970. The metal phase of Horse Creek, Mount Egerton, and Norton County enstatitic meteorites. Mineral. Mag. 37, 905–908.
Wasson, J.T., Wai, C.M., 1970. Composition of the metal, schreibersite and perryite of enstatite achondrites and the origin of enstatite chondrites and achondrites. Geochim. Cosmochim. Acta 34, 169–184.
Wasson, J.T., Kallemeyn, G.W., Rubin, A.E., 1994. Equilibration temperatures of EL chondrites: a major downward revision in the ferrosilite contents of enstatite. Meteoritics 29, 658–662.
Watters, T.R., Prinz, M., 1979. Their origin and relationship to enstatite chondrites. LPSC X, pp. 1073–1093.
Watters, T.R., Prinz, M., 1980. Mt. Egerton and the aubrite parent body. LPSC XI, pp. 1225–1227.
Watters, T.R., Prinz, M., Rambaldi, E.R., Wasson, J.T., 1980. ALHA 78113, Mt. Egerton and the aubrite parent body. Meteoritics 15, 386.
Wood, B.J., 2008. Accretion and core formation: constraints from metal–silicate partitioning. Phil. Trans. R. Soc. Lond. 366, 4339–4355.
Zerr, A., Diegeler, A., Boehler, R., 1998. Solidus of Earth's deep mantle. Science 281, 243–246.